

## ISTITUTO NAZIONALE DI RICERCA METROLOGICA Repository Istituzionale

One-dimensional photonic crystals with cylindrical geometry

*Original*

One-dimensional photonic crystals with cylindrical geometry / Roussey, Matthieu; Descrovi, Emiliano; Hänninen, Markus; Angelini, Angelo; Kuittinen, Markku; Honkanen, Seppo. - In: OPTICS EXPRESS. - ISSN 1094-4087. - 22:22(2014), pp. 27236-41-27241. [10.1364/oe.22.027236]

*Availability:*

This version is available at: 11696/63102 since: 2020-07-10T16:31:08Z

*Publisher:*

Optical Society of America

*Published*

DOI:10.1364/oe.22.027236

*Terms of use:*

This article is made available under terms and conditions as specified in the corresponding bibliographic description in the repository

*Publisher copyright*

Optical Society of America (OSA)

© Optical Society of America. One print or electronic copy may be made for personal use only. Systematic reproduction and distribution, duplication of any material in this paper for a fee or for commercial purposes, or modifications of the content of this paper are prohibited.

(Article begins on next page)

# One-dimensional photonic crystals with cylindrical geometry

Matthieu Roussey,<sup>1,\*</sup> Emiliano Descrovi,<sup>2</sup> Markus Häyrynen,<sup>1</sup> Angelo Angelini,<sup>2</sup>  
Markku Kuittinen,<sup>1</sup> and Seppo Honkanen<sup>1</sup>

<sup>1</sup>University of Eastern Finland, Institute of Photonics, 80101 Joensuu, P.O. Box 111, Finland

<sup>2</sup>Department of Applied Science and Technology, Politecnico di Torino, C.so Duca degli Abruzzi 24, 10129 Torino, Italy

\*matthieu.roussey@uef.fi

**Abstract:** A one-dimensional photonic crystal (1DPC) consisting of a stack of alternate TiO<sub>2</sub> and Al<sub>2</sub>O<sub>3</sub> layers is deposited on the side wall of a glass rod by Atomic Layer Deposition. The stack is designed to sustain TE-polarized Bloch Surface Waves (BSW) in the visible spectrum at wavelengths shorter than 650 nm. Experimental evidence of light coupling and guiding capabilities of the 1DPC is provided together with a possible application for fluorescence-based remote sensors.

©2014 Optical Society of America

**OCIS codes:** (310.1860) Deposition and fabrication; (240.6690) Surface waves; (050.5298) Photonic crystals; (060.2370) Fiber optics sensors.

---

## References and links

1. H. H. Hopkins and N. S. Kapany, "A flexible fibroscope using static scanning," *Nature* **173**(4392), 39–41 (1954).
2. B. Lee, "Review of the present status of optical fiber sensors," *Opt. Fiber Technol.* **9**(2), 57–79 (2003).
3. V. Bhatia and A. M. Vengsarkar, "Optical fiber long-period grating sensors," *Opt. Lett.* **21**(9), 692–694 (1996).
4. C. K. Kirkendall and A. Dandridge, "Overview of high performance fibre-optic sensing," *J. Phys. D Appl. Phys.* **37**(18), R197–R216 (2004).
5. O. S. Wolfbeis, "Fiber-optic chemical sensors and biosensors," *Anal. Chem.* **80**(12), 4269–4283 (2008).
6. W. Liang, Y. Huang, Y. Xu, R. K. Lee, and A. Yariv, "Highly sensitive fiber Bragg grating refractive index sensors," *Appl. Phys. Lett.* **86**(15), 151122 (2005).
7. X. Yang, F. Huo, H. Yuan, B. Zhang, D. Xiao, and M. M. F. Choi, "Sensitivity enhancement of fluorescence detection in CE by coupling and conducting excitation light with tapered optical fiber," *Electrophoresis* **32**(2), 268–274 (2011).
8. V. S. Afshar, S. C. Warren-Smith, and T. M. Monro, "Enhancement of fluorescence-based sensing using microstructured optical fibres," *Opt. Express* **15**(26), 17891–17901 (2007).
9. F. Vollmer, D. Braun, A. Libchaber, M. Khoshshima, I. Teraoka, and S. Arnold, "Protein detection by optical shift of a resonant microcavity," *Appl. Phys. Lett.* **80**(21), 4057 (2002).
10. X. Fan, I. M. White, S. I. Shopova, H. Zhu, J. D. Suter, and Y. Sun, "Sensitive optical biosensors for unlabeled targets: A review," *Anal. Chim. Acta* **620**(1-2), 8–26 (2008).
11. K. T. V. Grattan and T. Sun, "Fiber optic sensor technology: an overview," *Sens. Actuators* **82**(1-3), 40–61 (2000).
12. R. Jarzebinska, E. Chehura, S. W. James, and R. P. Tatam, "Multiplexing a serial array of tapered optical fibre sensors using coherent optical frequency domain reflectometry," *Meas. Sci. Technol.* **23**(10), 105203 (2012).
13. D. Paladino, A. Iadicco, S. Campopiano, and A. Cusano, "Not-lithographic fabrication of micro-structured fiber Bragg gratings evanescent wave sensors," *Opt. Express* **17**(2), 1042–1054 (2009).
14. J. P. Parry, B. C. Griffiths, N. Gayraud, E. D. McNaghten, A. M. Parkes, W. N. MacPherson, and D. P. Hand, "Towards practical gas sensing with micro-structured fibres," *Meas. Sci. Technol.* **20**(7), 075301 (2009).
15. B. Lee, S. Roh, and J. Park, "Current status of micro- and nano-structured optical fiber sensors," *Opt. Fiber Technol.* **15**(3), 209–221 (2009).
16. K. O. Hill and G. Meltz, "Fiber Bragg grating technology fundamentals and overview," *J. Lightwave Technol.* **15**(8), 1263–1276 (1997).
17. Y. Zhao, F. Pang, Y. Dong, J. Wen, Z. Chen, and T. Wang, "Refractive index sensitivity enhancement of optical fiber cladding mode by depositing nanofilm via ALD technology," *Opt. Express* **21**(22), 26136–26143 (2013).
18. A. Cusano, A. Iadicco, P. Pilla, A. Cutolo, M. Giordano, and S. Campopiano, "Sensitivity characteristics in nanosized coated long period gratings," *Appl. Phys. Lett.* **89**(20), 201116 (2006).
19. L. L. Xue and L. Yang, "Sensitivity Enhancement of RI Sensor Based on SMS Fiber Structure with high refractive index overlay," *J. Lightwave Technol.* **30**(10), 1463–1469 (2012).
20. M. Jiang, Q. S. Li, J. N. Wang, Z. Jin, Q. Sui, Y. Ma, J. Shi, F. Zhang, L. Jia, W. G. Yao, and W. F. Dong, "TiO<sub>2</sub> nanoparticle thin film-coated optical fiber Fabry-Perot sensor," *Opt. Express* **21**(3), 3083–3090 (2013).

21. M. H. Tu, T. Sun, and K. T. V. Grattan, "Optimization of gold-nanoparticle-based optical fibre surface plasmon resonance (SPR)-based sensors," *Sens. Actuators B Chem.* **164**(1), 43–53 (2012).
22. P. Yeh, A. Yariv, and A. Y. Cho, "Optical surface waves in periodic layered media," *Appl. Phys. Lett.* **32**, 104 (1978).
23. W. M. Robertson, "Experimental measurement of the effect of termination on Surface Electromagnetic Waves in one-dimensional photonic bandgap arrays," *J. Lightwave Technol.* **17**(11), 2013–2017 (1999).
24. E. Descrovi, T. Sfez, L. Dominici, W. Nakagawa, F. Michelotti, F. Giorgis, and H. P. Herzig, "Near-field imaging of Bloch surface waves on silicon nitride one-dimensional photonic crystals," *Opt. Express* **16**(8), 5453–5464 (2008).
25. M. Liscidini, M. Galli, M. Shi, G. Dacarro, M. Patrini, D. Bajoni, and J. E. Sipe, "Strong modification of light emission from a dye monolayer via Bloch surface waves," *Opt. Lett.* **34**(15), 2318–2320 (2009).
26. M. Ballarini, F. Frascella, F. Michelotti, G. Digregorio, P. Rivolo, V. Paeder, V. Musi, F. Giorgis, and E. Descrovi, "Bloch surface waves-controlled emission of organic dyes grafted on a one-dimensional photonic crystal," *Appl. Phys. Lett.* **99**(4), 043302 (2011).
27. E. Descrovi, F. Frascella, M. Ballarini, V. Moi, A. Lamberti, F. Michelotti, F. Giorgis, and C. F. Pirri, "Surface label-free sensing by means of a fluorescent multilayered photonic structure," *Appl. Phys. Lett.* **101**(13), 131105 (2012).
28. M. Ballarini, F. Frascella, N. De Leo, S. Ricciardi, P. Rivolo, P. Mandracci, E. Enrico, F. Giorgis, F. Michelotti, and E. Descrovi, "A polymer-based functional pattern on one-dimensional photonic crystals for photon sorting of fluorescence radiation," *Opt. Express* **20**(6), 6703–6711 (2012).
29. R. Badugu, K. Nowaczyk, E. Descrovi, and J. R. Lakowicz, "Radiative decay engineering 6: fluorescence on one-dimensional photonic crystals," *Anal. Biochem.* **442**(1), 83–96 (2013).
30. R. Ulrich, "Theory of the prism-film coupler by plane wave analysis," *J. Opt. Soc. Am.* **60**(10), 1337–1350 (1970).
31. V. Miikkulainen, M. Leskelä, M. Ritala, and R. L. Puuronen, "Crystallinity of inorganic films grown by atomic layer deposition: Overview and general trends," *J. Appl. Phys.* **113**(2), 021301 (2013).
32. S. Fiorilli, P. Rivolo, E. Descrovi, C. Ricciardi, L. Pasquardini, L. Lunelli, L. Vanzetti, C. Pederzoli, B. Onida, and E. Garrone, "Vapor-phase self-assembled monolayers of aminosilane on plasma-activated silicon substrates," *J. Colloid Interface Sci.* **321**(1), 235–241 (2008).

## 1. Introduction

Since several decades, optical fibers are used as sensors [1–5]. Indeed, they offer a long interaction length with bulky analytes, which makes them very efficient sensors. A large panel of optical fiber based sensors exists, enabling the measurement of refractive index variations with a resolution as high as  $10^{-5}$  RIU [6], the detection of fluorescence signals with a limit of detection of a few nanomols [7,8], or allowing the monitoring of bio-chemical activities or reactions [9,10]. There are mainly three types of sensors based on fiber optics: the point sensor, where the tip of the fiber is the only sensing part; the distributed sensor, where the sensing involves the whole fiber length; and the quasi-distributed sensor, which is a compromise between the two others [11]. The operating principle of such a sensor is to modify the behavior of the propagating light within the fiber through the variation of the external medium properties. Any change in the external medium is sensed by the evanescent field associated to the fiber modes. In order to increase the sensitivity, the overlap between the evanescent wave and the external medium should be maximized. To this end, several solutions have been proposed along the years, by tapering [12,13] or micro-structuring the fiber [14], by creating a Bragg reflector inside the fiber [15,16], or by adding either a coating [17–19] or particles around the fiber [20,21].

Here we propose a novel and low-cost approach to increase the Local Density of States (LDOS) at the surface of a cylindrical transparent rod, based on the concept of Bloch Surface Waves sustained on dielectric multilayers (also called a one-dimensional photonic crystal, 1DPC). BSW are electromagnetic modes with either TE or TM polarization that can be coupled in a properly designed 1DPC [22–24]. Thanks to the surface-bound nature of these modes, the corresponding intensity maximum is located close to the 1DPC surface, where field enhancement effects occur. Similarly to the well-known Surface Plasmon Coupled Emission (SPCE), the surface confinement of the electromagnetic energy associated to BSW provides a high LDOS that ultimately drains a significant fraction of radiated power from emitters located on the 1DPC surface [25–29]. In the following we provide an experimental evidence of BSW-coupled emission in a 1DPC that is conformational to a large cylindrical glass bar.

Figure 1(a) schematically illustrates a cross-sectional view of a cylindrical 1DPC. When a dipolar emitter is located close to the 1DPC surface, its corresponding angular radiative pattern is altered upon the coupling within the available modes. In our case, since a TE-polarized BSW is supported by the 1DPC, a dipolar emitter having its dipole momentum lying tangentially to the cylindrical side wall will couple a significant portion of its radiated energy therein. Such a BSW-coupled emission will then leak within the glass substrate after having travelled on the 1DPC surface for a characteristic propagation length. The leakage angle  $\theta_{\text{BSW}}$  depends on the emission wavelength as specifically determined by the BSW dispersion curve [26], in such a way that the wavevector component parallel to the cylindrical glass is conserved. As shown in Fig. 1(a), the leakage angle is larger than the critical angle  $\theta_c$  for the air/glass interface. The presence of the 1DPC definitely alters the radiation pattern of the emitting dipole. In fact, if we consider the case of a bare glass surface (Fig. 1(b)) [26], most of the radiated energy is emitted within an angular range falling below the critical angle.

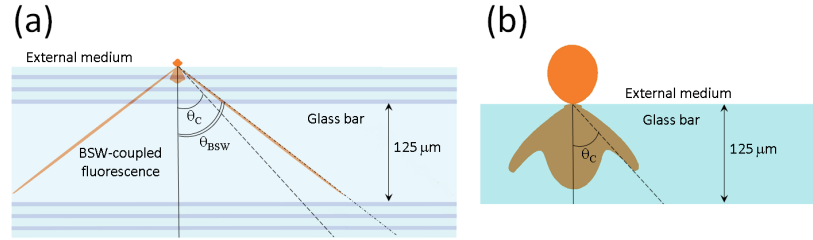


Fig. 1. (a) Angular radiative pattern of a dipolar emitter on a 1DPC deposited on glass substrate. The dipole has its dipole momentum oriented normally to the figure plane. The BSW-coupled emission is leaking into the substrate according to a two-lobed distribution at angles larger than the critical angle for the air/glass interface; (b) angular radiative pattern of a dipolar emitter oriented as in case (a), located on a bare glass surface.

In order to implement this configuration, the main challenge is then the deposition of the 1DPC around the rod. Two materials are involved in order to create the photonic crystal structure. Each layer must have a well-defined thickness homogeneously deposited. Recently, Zhao *et al.* [17] have shown that Atomic Layer Deposition (ALD) is an ideal technique to perform this task, by creating a layer of aluminum oxide ( $\text{Al}_2\text{O}_3$ ) around a glass bar. We propose here to extend this technique for the fabrication of the required cylindrical 1DPC.

## 2. Design and fabrication

The 1DPC is a stack of a high refractive index material (titanium dioxide,  $\text{TiO}_2$ ) and a low index material (aluminum oxide,  $\text{Al}_2\text{O}_3$ ). The refractive indices of these two amorphous materials at the wavelength  $\lambda = 532$  nm are  $n_{\text{TiO}_2} = 2.32$  and  $n_{\text{Al}_2\text{O}_3} = 1.64$ , as measured by ellipsometry. The cylindrical photonic structure can be locally considered as flat, because of the rather large diameter ( $125 \mu\text{m}$ ) of the silica bar. For this reason, the 1DPC design can be performed by using a conventional Transfer Matrix Method for planar multilayers. In the present case, the stack is constituted by 6 pairs of high and low-index materials, as follows: substrate- $[\text{TiO}_2\text{-Al}_2\text{O}_3] \times 6$ -air. From design, the  $\text{Al}_2\text{O}_3$  layer is 150 nm thick while the  $\text{TiO}_2$  layer is 80 nm thick. However, on the experimental side, the real thicknesses obtained are 146 nm and 81 nm for the  $\text{Al}_2\text{O}_3$  and the  $\text{TiO}_2$  layers, respectively.

This 1DPC can sustain TE-polarized BSW, as shown in the calculated angularly-resolved reflectivity map reported in Fig. 2(a). In the computational model, the actual layer thicknesses are used and an absorption coefficient  $k = 3 \cdot 10^{-4}$  (estimated by ellipsometry on ALD-deposited films of  $\text{Al}_2\text{O}_3$  and  $\text{TiO}_2$ ) is introduced in the refractive index of the ALD-grown layers. The BSW dispersion line corresponds to the narrow low-reflectivity line running beyond the critical angle. From the reflectivity dip width it is indeed possible to extract an estimation of the BSW propagation length  $L_{\text{BSW}}$ , according to the relationship  $L_{\text{BSW}} = (\pi\sigma/\lambda_{\text{BSW}})^{-1} = 109 \mu\text{m}$ , where  $\sigma$  is the full width at half maximum bandwidth (FWHM) of the BSW reflectivity dip and  $\lambda_{\text{BSW}}$  is the BSW wavelength [see the inset in Fig. 2(a)] [30]. In Fig.

2(b), the cross sectional BSW intensity distribution is shown. It should be noted that the BSW high energy density is produced at the distal surface of the 1DPC.

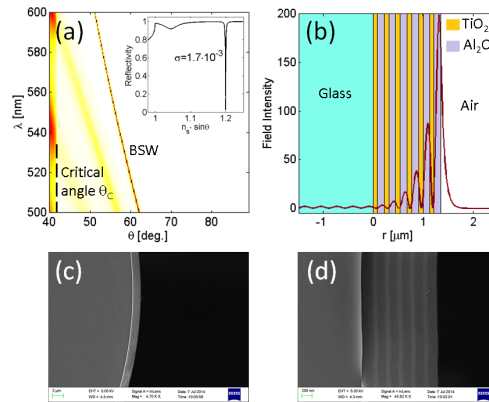


Fig. 2. (a) TE-polarized reflectivity map of a 1DPC as illuminated from the glass substrate, (inset) reflectivity profile at  $\lambda = 580$  nm; (b) cross-sectional BSW intensity distribution across the 1DPC; (c,d) SEM images of side walls of a cleaved facet of a 1DPC-coated glass bar.

The 1DPC is fabricated by Atomic Layer Deposition (ALD) on silica bars of a diameter of 125  $\mu\text{m}$  that are customized and produced by Oplatek Group Oy, especially for this purpose. These bars have no cladding and are highly multimodal in nature. ALD is a unique thin film deposition cycling technique, based on saturative reactions of alternately supplied precursor vapors. The use of vapors and self-terminating reactions provides to ALD rare benefits such as a very accurate control of the film thickness, a high quality of the films in terms of surface roughness and homogeneity, a conformal deposition over large areas, and a perfect step coverage [31]. These advantages have aroused increasing interest toward ALD in photonics applications.

In order to assure a homogeneous coating all around the substrate, the silica bar is propped from edges, so it is hanging in air. Moreover, the bars are placed perpendicular to the gas flow in the chamber in order to obtain a uniform coating over the whole length of the bar (about 12 cm). The ALD process used in this experiment is thermal-based at a temperature of 120°C. To avoid any delaminating during the deposition, the bars are placed in the reaction chamber 12h in advance in order to stabilize the temperature and confirm that the bars and the reactor are at the same temperature during the coating process.

$\text{TiO}_2$  layers were grown by using titanium tetrachloride ( $\text{TiCl}_4$ ) and water ( $\text{H}_2\text{O}$ ) as precursors and  $\text{Al}_2\text{O}_3$  layers by using trimethyl aluminum (TMA) and water as precursors with ALD TFS 200 equipment by Beneq.

Figures 2(c) and 2(d) show SEM pictures of the cleaved bars. Note that even if the coating is relatively robust, the cleaving process may lead to a delaminating of the stack from the glass bar. Several attempts are usually needed before obtaining a homogeneous output end of the bar. From the large view on Fig. 2(c), one can see the perfect conformal and homogeneous coating of the silica bar, and from Fig. 2(d), it is possible to confirm the thickness of the different layers forming the stack. They have been measured as 81 nm for the  $\text{TiO}_2$  layers and 146 nm for the  $\text{Al}_2\text{O}_3$  layers. One can remark also that the thickness is well controlled over all the six periods composing the film stack. This is possible only if the temperature of the process is stabilized before the deposition. We indeed remark that, if the deposition is started before the temperature of the substrate (the cylindrical bar in this case) reaches the chamber's one, the first layers are thinner, as compared to the expected values.

### 3. Fluorescence coupling and guiding

In order to investigate the capabilities of the 1DPC-coated glass rod to couple and guide fluorescence radiation from external emitters through BSW, a homogeneous layer of

Rhodamine 6G has been adsorbed on the 1DPC surface. Thanks to the close proximity of R6G molecules to the 1DPC, a near-field coupling of the radiated power occurs in the BSW mode at the corresponding emission wavelengths of the dye [29]. Fluorescence is excited by a frequency doubled Nd:YAG laser ( $\lambda = 532$  nm) focused perpendicularly to the bar axis, as shown in the sketch of Fig. 3(a). Focusing is performed by a cylindrical lens providing a rather homogeneous illumination along the bar transverse cross-section, with a spot spread over roughly  $10\text{ }\mu\text{m}$  in the direction of the bar axis. For comparison purposes, a bare glass rod is also employed in a similar fashion. The laser excitation can be provided at different distances from the bar facet by scanning the focusing stage. The bar facet is imaged on a CCD by means of an NA = 0.2 objective through an edge filter (RazorEdge® Longpass 532) for filtering out all laser radiation that is eventually collected.

Exemplary false-color images of fluorescence leaking out of the 1DPC-coated bar facet are shown in Figs. 3(b)-3(d) for several laser excitation positions, as indicated. Some defects on the bar facet (probably due to cleaving) appear as bright scattering spots. When the laser excitation position is close to the bar facet, a bright fluorescent ring is detected [Fig. 3(b)]. The bright ring corresponds to light guided into the 1DPC after a resonant coupling of R6G molecules with the BSW mode. At short excitation distances from the bar facet, the observed BSW-coupled fluorescence is still tightly confined within the 1DPC, and is thus propagated to the collection optics mainly from the coated side walls of the bar. When the laser excitation position is brought far away from the bar facet, fluorescence starts to appear also in the inner portion of the bar. Therefore, a general decrease of the intensity contrast between the 1DPC and the bar inner part is observed. We ascribe this effect to the leakage of BSW-coupled fluorescence from the 1DPC surface into the glass core, where it is guided according to the sketch in Fig. 1(a). The bright fluorescent ring at the bar end facet is only observed for the 1DPC-coated case, while the bare glass bar fluorescence is homogeneously distributed, as shown in Fig. 3(e), regardless of the laser excitation position. We ascribe this observation to the highly multimodal nature of the glass bar.

A set of fluorescence images of the 1DPC-coated bar facet is collected for different laser excitation positions in the range  $[50\text{ }\mu\text{m} - 2000\text{ }\mu\text{m}]$  at a  $50\text{ }\mu\text{m}$  step. Each image is individually normalized to its maximum of intensity. Then, an average intensity is calculated over three different regions selected within the normalized intensity images. The three regions include two circular portions of the rod side walls comprising the 1DPC and an inner central portion, respectively, as indicated by the rectangular boxes in the inset of Fig. 3(f). Then, the ratio of the average intensity associated to the 1DPC over the average intensity associated to the rod inner region is calculated for each collected image. Such an intensity ratio is plotted as a function of the laser excitation distance  $z$  in Fig. 3(f). Starting from an initial condition at  $z = 50\text{ }\mu\text{m}$  where the fluorescence intensity at the 1DPC coating is roughly one order of magnitude higher as compared to the bar inner part, a monotonic decrease of the contrast is observed. Asymptotically, the fluorescence contrast tends to a unitary value, meaning that no preferential guiding is observed along the 1DPC with respect to the bar inner region.

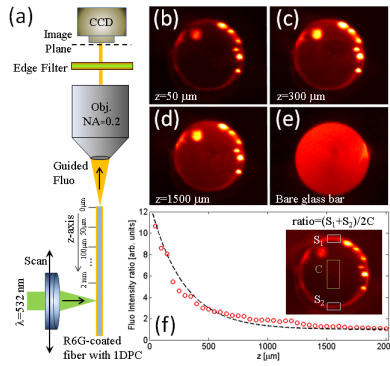


Fig. 3. (a) Experimental setup; (b-d) exemplary fluorescence images of the 1DPC-coated end facet upon laser excitation at different excitation distances, as indicated therein. The bright spots are due to fluorescence scattering from 1DPC cracks on the facet; (e) fluorescence image of the cleaved facet of a bare glass bar; (f) ratio of the fluorescence intensity averaged over the two side wall regions  $S_1$  and  $S_2$  over the fluorescence intensity averaged in the inner region C (inset) as a function of the laser excitation position. Experimental data (red circles) are well fitted by an exponential curve (dashed line) having a 250  $\mu\text{m}$  decay constant.

The fluorescence contrast curve is well fitted by an exponential function having a decay constant of 250  $\mu\text{m}$ . The decay constant provides an indication on the length travelled by the BSW-coupled fluorescence within the 1DPC before leaking into the glass bar. The experimental value is larger than the propagation length  $L_{\text{BSW}} = 109 \mu\text{m}$  as estimated from the 1DPC design. This effect can be explained by invoking a re-coupling mechanism back into the 1DPC after multiple reflections at the bar sidewalls. Basically, the BSW-coupled fluorescence leaked into the substrate can partially tunnel through the 1DPC and couple back to a BSW mode after being reflected at opposite sidewalls. This effect can occur thanks to the narrow angular dispersion of the BSW-coupled fluorescence, as sketched in Fig. 1(a). As a consequence, fluorescence can be propagated within the 1DPC for an overall distance that is larger than the propagation length of the mode expected from calculations.

#### 4. Conclusion

We demonstrated the fluorescence coupling and guiding capabilities of a one-dimensional photonic crystal with cylindrical geometry, fabricated on a glass rod. Although the design constraints for a 1DPC to be able to sustain surface modes are rather stringent, we managed to obtain a highly conformal multilayer on a cylindrical substrate by means of the ALD technique. We indeed exploited several unique advantages of the ALD, such as the conformal coating over non-flat surfaces and the accurate control of the film thickness.

Moreover, these results prove the potential of such kind of a platform for the realization of fibered fluorescence sensors with high throughput. Indeed, the multilayer is fully compatible with the above mentioned fiber optic based sensors, in particular, tapered fibers. In addition, the last alumina layer can be decorated by metallic nanoparticles for Raman enhanced detection schemes. We finally point out that other materials can be used for tailoring the 1DPC, such as silica instead of alumina, thus allowing well-known functionalization routes to be used (e.g. based on organo-silanes [32]).

#### Acknowledgments

This research has received funding from the EU FP7 project BILOBA (Grant # 318035) and is supported by the Finnish Funding Agency for Technology and Innovation (TEKES) through the Fidipro-project NP-nano and the EAKR projects ALD-nano-medi and Nanobio (grants 70011/12 and 70005/14) and the Academy of Finland (grants 272155 and 250968). The authors wish to thank Oplatek Group Oy for providing the silica bars.